Chemical Engineering Journal 487 (2024) 150722

Contents lists available at ScienceDirect

Chemical Engineering Journal

journal homepage: www.elsevier.com/locate/cej

Modeling the temperature-programmed reduction of metal oxide catalysts by considering the particle-size distribution effect

Jhonny Villarroel-Rocha [a,b], Antonio Gil [a,*]

[a] INAMAT˜2, Departamento de Ciencias, Universidad Pública de Navarra, Campus de Arrosadía, 31006 Pamplona, Spain
[b] Laboratorio de Sólidos Porosos, Instituto de Física Aplicada, CONICET, Universidad Nacional de San Luis, 5700 San Luis, Argentine

ARTICLE INFO

Keywords:
Metal oxides
Temperature-programmed reduction
Particle-size distribution
Solid-state reaction kinetic models

ABSTRACT

Hydrogen temperature-programmed reduction (H_2-TPR) has become a very useful and common technique for the chemical characterization of solids as it is sensitive to the study of reducible species in catalysis and is considered to be a fingerprint for the reducibility of metal oxide catalysts. However, although modeling of H_2-TPR patterns has been extensively studied, little attention has been paid to the effect of particle-size distribution (PSD). The complexity of modeling H_2-TPR patterns arises from the fact that the chemistry of metal oxide reduction depends on several factors, including particle size, nature of the support material and confinement within the porous structure, amongst others. In order to identify the kinetic reaction model governing the reduction of certain metal oxides and to explore the effect of PSD, pure metal oxides that only exhibited the particle size difference effect were used to model the H_2-TPR patterns. Kinetic and thermodynamic data, which are very useful for characterizing heterogeneous catalysts, were obtained from this study. This work presents a simple procedure for modeling H_2-TPR patterns of various metal oxides (i.e., CuO, Ag_2O, and NiO) used as active phases in several reactions of environmental and energetic interest using several solid-state reaction kinetic models and considering their PSDs. The results obtained show that modeling the H_2-TPR profiles provides information regarding the PSD of metal oxide catalysts that undergo a single-step reduction and only present the particle size difference effect.

1. Introduction

The development of new materials implies that they must be characterized using several experimental techniques. Some of the most important such techniques are those involving thermal analysis, including thermogravimetric analysis (TGA), differential thermal analysis (DTA), differential scanning calorimetry (DSC), and temperature programmed analyses (TPX), amongst others. These techniques allow various thermal and kinetic parameters—including thermal stability, determination of degradation/decomposition temperatures, and oxidation/reduction or transition steps—to be determined.

Among the thermal analysis techniques mentioned, temperature-programmed reduction (TPR) has become a very useful and common method for the chemical characterization of solids as it is sensitive to the study of reducible species in catalysis. This technique is frequently used quantitatively to obtain information on the effect of support materials, the reduction steps, the amount of reducible species and the temperature at which the maximum rate occurs [1]. However, TPR can also be used quantitatively to determine: *i)* the quantity of reducible species present in the solid catalyst and the oxidation state; *ii)* the correct form of the kinetic reduction model; and *iii)* the kinetic parameters (activation energy and pre-exponential factor of the rate constant) [2–17]. For these reasons, the experimental H_2 temperature-programmed reduction (H_2-TPR) pattern is considered to be a fingerprint for the reducibility of the catalyst. The principle of the TPR technique is the reduction of a metal oxide present in a solid catalyst with a flowing gas (commonly H_2) while simultaneously increasing the temperature of the system in a predetermined way [5,18], thus resulting in reduction of the metal under non-isothermal conditions. Chemical information can then be derived by analyzing the gaseous products. The reduction of the metal oxide that occurs in a TPR analysis is, therefore, a heterogeneous solid-state (solid–gas) reaction, which means that the mechanism of the reaction and the kinetic parameters can be determined by combining the experimental TPR data with the theory of reaction kinetic models [19].

Many mathematical equations for reaction kinetic models have been proposed to relate the type of rate mechanisms, including: i) geometrical

* Corresponding author.
E-mail address: andoni@unavarra.es (A. Gil).

https://doi.org/10.1016/j.cej.2024.150722
Received 12 October 2023; Received in revised form 19 February 2024; Accepted 25 March 2024
Available online 26 March 2024

contraction models [20,21]; ii) diffusion models [20,22–31]; and iii) nucleation and nuclei growth models [32,33]. Although all reaction kinetic models proposed to date were derived for particles of identical size, solid reactants always present particle-size distribution (PSD), which has been shown to have a significant effect on the course of a solid-state reaction. For this reason, it is important that those simple reaction kinetic models can consider the effect of the PSD of the solid reactant in order to achieve a system as close to reality as possible (e.g., the smaller particles will be consumed in a shorter period of time than their larger counterparts). Therefore, the reaction rate per unit area or volume, which is based on the diameter of an individual particle, will be affected. Furthermore, in the field of materials science and technology, it is well-established that metal oxide catalysts undergo significant alterations in their physical and chemical properties with particle size. Various studies suggest that metal and metal oxide particles, as they approach nanoscale dimensions, experience substantial changes, particularly in the interactions occurring at this scale. This is attributed to the higher surface-to-volume ratio, facilitating enhanced contact between reactive species and potentially prolonging their interaction. Consequently, these nanoparticles exhibit unique and improved catalytic responses compared to larger particles. This underscores the importance of controlling and characterizing particle size distribution, especially in catalyst design, particularly in fields such as heterogeneous catalysis, aiming for enhanced selectivity, reactivity, and stability.

In this sense, various methodologies that consider the PSD of the reactive solid have been reported [6,34–49]. However, in most cases, it is necessary to use complex mathematics, which makes them difficult to apply. In addition to this mathematical complexity, the proposed methodology, regardless of which one is used, will not provide an exact analytical solution, which explains why numerical and approximation methods have been used to solve this problem.

Although various solid-state reactions have been studied using several reaction kinetic models, and, specifically, H_2-TPR pattern modeling [5–11,50–57], of these reports only Tonge [6] considered the effect of PSD by applying a geometrical contraction model for NiO reduction, concluding that the kinetic model mostly fails to reproduce the experimental data. The complexity of modeling H_2-TPR patterns is due to the fact that the chemistry of metal oxide reduction depends on particle size, support material, and confinement within pores. Furthermore, in addition to PSD, other factors affect the reduction chemistry of metal oxide catalysts, such as [1,5,18]: *i)* the chemical composition (nature of metals and metal oxides in the catalyst); *ii)* the shape of metal oxide particles (exposure of different crystal faces and the presence of surface defects can impact reactivity); *iii)* the specific surface area (increasing the available surface area enhances interaction with the reducing gas); and *iv)* the presence of co-catalysts (the presence of other elements in the material can modify the kinetics of reduction and the formation of gaseous products).

Considering the aforementioned, it is important to note that while nanoparticles exhibit unique reaction mechanisms compared to their macroscale counterparts in bulk materials, to achieve a comprehensive understanding of the impact of particle size on the reducibility of metal oxide catalysts with H_2, it is essential to first comprehend their behavior in bulk materials. Thus, subsequently, after generating the necessary fundamental theoretical knowledge, advancements can be made in mathematical modeling, incorporating metal oxide catalysts with nanoscale particle sizes.

As such, in order to identify the reaction kinetic model governing the reduction of certain metal oxides and to study the effect of PSD, pure metal oxides could be used to model their H_2-TPR patterns. This study will provide kinetic and thermodynamic data that can be very useful for characterizing the solid catalyst. This work presents an easy methodology that combines the theory of kinetic analyses for solid-state reactions with PSD analyses with the aim of modeling H_2-TPR patterns for various metal oxides (i.e., CuO, Ag_2O and NiO). These oxides have been selected for two reasons: because the H_2 consumption in the reduction process is performed in a single stage, and because they are active metallic phases for energetic and environmental applications of great interest in processes such as hydrogenation, reforming and bactericides, amongst others.

2. Experimental

2.1. Materials

The metal oxide powders used in the study were: copper(II) oxide (Aldrich, 99.995 %), silver(I) oxide (Aldrich, 99.99+ %) and nickel(II) oxide. The NiO powder was obtained by thermal decomposition of Ni$(NO_3)_2{\cdot}6H_2O$ (Alfa Aesar, 98 %) at 670 K (in air) for 4 h at a heating rate of 5 K·min^{-1}.

2.2. Characterization of metal oxides

The metal oxides were characterized by powder X-ray diffraction (XRD) in a Bruker D8 Advance ECO diffractometer, using Cu-Kα radiation, between 10° and 70° (2θ), with a scanning rate of 2°·min^{-1}. The average crystallite sizes (D) of the metal oxides were calculated from the XRD data using the Scherrer formula [58] shown in Eq. (1):

$$D = \frac{K^* \bullet \lambda}{\Delta \bullet cos(\theta)} \quad (1)$$

where K^* is the shape factor (0.9), λ is the X-ray wavelength of Cu-Kα radiation (0.15406 nm), and Δ is the full width at half maximum (FWHM, in rad) of the respective reflection at the Bragg angle θ (in rad).

The morphology and particle sizes of the samples were studied by scanning electron microscopy (SEM) using Inspect-F50 equipment. The micrographs taken by this equipment correspond to projected areas whose dimensions depend on the orientation of the particles on the slide. Since particles in a stable orientation tend to present their maximum area (neglecting the smaller dimensions of the particles), generally, the particle sizes obtained by SEM tend to be larger than those measured by other techniques [59]. This makes particle size measurements obtained by microscopy orientation-dependent (known as statistical diameters). Therefore, to obtain a statistically acceptable measurement, it is necessary to perform several particle size measurements (chosen randomly) and subsequently represent them in a distribution. Of the different methods for estimating particle size, the most representative for both spherical and non-spherical particles is the projected area diameter or equivalent diameter (which is the diameter of a circle that has the same projected area as the particle).

SEM micrographs of the metal oxides were taken at magnifications between 1000x and 100000x with the aim of identifying all particles present in a size range between 0.05 and 50 μm. Once the particle sizes were identified, ImageJ software (v. 1.54d) was used to determine the PSD based on SEM images (with a set of three and six images for each sample in order to obtain between 300 and 600 particles) with the appropriate magnification for this purpose. Specifically, the magnifications used were 5000x for CuO (Fig. 1S), 20000x for Ag_2O (Fig. 2S) and 100000x for NiO (Fig. 3S). The particle sizes (d_p) of the samples under study, with spherical and non-spherical morphologies, were estimated using the definition of equivalent diameter (considering that the diameter of a circle has the same area, S_p, as the particle projection) represented by Eq. (2).

$$d_p = \sqrt{\frac{4 \bullet S_p}{\pi}} \quad (2)$$

In addition, the ImageJ software was used to determine the circularity value of particles to assess the distribution of particle shapes of the solid. A circularity value of 1 indicates a perfect circle, and as the value approaches 0, it indicates an increasingly elongated polygon.

H_2-TPR measurements were performed using a Micromeritics TPR/

TPD 2900 instrument equipped with a thermal conductivity detector (TCD). About 15 mg of metal oxide was placed inside a quartz U-tube, pretreated under a He flow of 40 STP $cm^3 \cdot min^{-1}$ at 373 K for 1 h, and subsequently cooled to room temperature. The reduction was then performed from room temperature until metal reduction was complete at several nominal heating rates (β) of between 6 $K \cdot min^{-1}$ (0.1 $K \cdot s^{-1}$) and 18 $K \cdot min^{-1}$ (0.3 $K \cdot s^{-1}$), under a 5 % H_2 in Ar purified carrier (Nippon Gases) at a flow rate of 40 STP $cm^3 \cdot min^{-1}$. These experimental conditions were selected based on the recommendations published by Monti-Baiker [12] and Malet-Caballero [60]. The TPR tests for each sample at each nominal heating rate were performed two or three times, resulting in a very reproducible data with an accuracy of the maximum position of the TPR peak of ± 5 K, as shown in Fig. 4S. The experimental reduction degree curve (α) vs reaction temperature (T) was determined by integrating the H_2 consumption provided by the TCD signals of the H_2-TPR data according to Eq. (3):

$$\alpha = \frac{F_{[T_0,T]}}{F_{[T_0,T_F]}} \tag{3}$$

where $F_{[T_0,T]}$ is the reduction area corresponding to partial reduction in the temperature range from T_0 (initial temperature of the TPR analysis) to a given partial temperature T, and $F_{[T_0,T_F]}$ is the total reduction area from T_0 to final temperature (T_F) at which the metal oxide reduction finished.

3. Mathematical modeling of TPR patterns

The present mathematical modeling considers only macroscopic information (such as the PSD), with the limitation that it does not include microscopic information (such as atomic details) about the surface of the particle. Therefore, modeling of H_2-TPR profiles was carried out by performing a kinetic study of the reduction of the metal oxides involving various solid-state kinetic models and also considering the PSD of the oxide. Here, the metal oxide particles were considered as spherical particles of diameter d_p, with the corresponding particle volume (V_p) being obtained by:

$$V_p = \frac{\pi}{6} \bullet {d_p}^3 \tag{4}$$

As reduction of the metal oxide occurs, the unreduced particle volume (V) can be expressed as a function of degree of reduction (α), as follows:

$$V = \frac{\pi}{6} \bullet {d_p}^3 \bullet (1-\alpha) \tag{5}$$

As such, the reduction reaction rate, i.e. the rate of decrease of the unreduced particle volume ($-\left(\frac{1}{V_p}\right)\frac{dV}{dt}$), or the rate of increase of the reduced particle volume, derived from Eq. (5), is given by:

$$-\left(\frac{1}{V_p}\right)\frac{dV}{dt} = \frac{d\alpha}{dt} \tag{6}$$

The term $-\left(\frac{1}{V_p}\right)\frac{dV}{dt}$ in eq. (6) is directly proportional to the hydrogen consumed during the reduction. Therefore, considering this term as a function of the reaction temperature (T), the $-\left(\frac{1}{V_p}\right)\frac{dV}{dt}$ vs T profile can be directly related to the experimental H_2-TPR data (i.e., TCD signal vs T). In this sense, it is crucial to have an adequate reaction model that accurately represents the metal oxide-H_2 system and establishes a relationship between the degree of reduction and the reaction temperature.

3.1. Solid-state reaction kinetic models

The reaction kinetic models considered in this work were geometrical contraction, diffusion, and nucleation. Scheme 1 schematically represents these models for the reduction process of a spherical metal oxide particle, where a detailed explanation of the reduction mechanism for each of them is provided below.

3.1.1. Geometric contraction models

In this type of reaction kinetic model, the nucleation process and diffusion of the reactants through the product layer are fast, thus resulting in the formation of a homogeneous layer of product that covers the entire metal oxide particle, as shown in Scheme 1a for a spherical particle. Moreover, the reaction interface decreases as the reaction progresses [13]. Therefore, in geometric contraction models the chemical reaction is controlled by the surface or phase boundary (reaction interface), and these can be derived assuming particles with a well-defined geometry. The mathematical equations included in this group are the contracting area model for a cylindrical particle [21] and contracting volume model for a spherical particle [20]. Specifically, in reduction reactions, the contracting volume model has been employed in the reduction of nickel oxide [6], copper oxide [52], silver oxide [51], iron oxide [9], and other metal oxides [5]. The contracting volume (CV) model is given by Eq. (7):

$$1-(1-\alpha)^{\frac{1}{3}} = \frac{k \bullet t}{\left(\frac{d_p}{2}\right)} \tag{7}$$

where k (in $m \cdot s^{-1}$) is the reaction constant and t is the reaction time (in s).

In the present work, the contraction volume equation was used as the geometrical contraction model.

3.1.2. Diffusion models

Diffusion models assume that a thin homogeneous layer of product is formed around the particle at the beginning of the reaction, as is the case

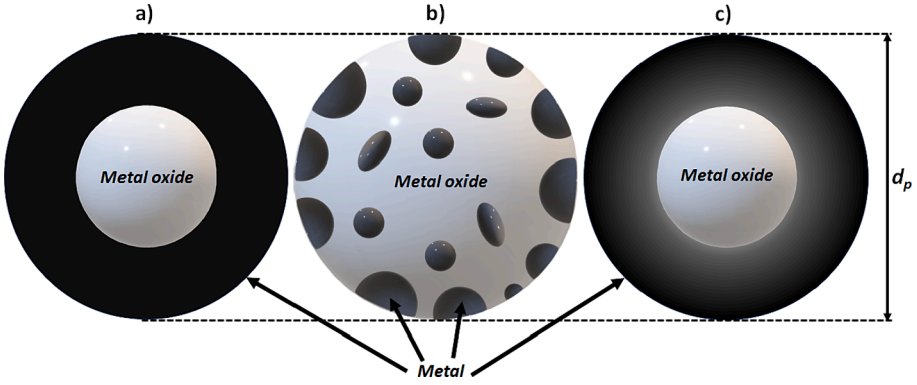

Scheme 1. Schematic models of the reduction of a metal oxide particle: a) geometric contraction, b) nucleation and c) diffusion models.

with the geometric contraction models. However, as the chemical reaction progresses, it is limited by diffusion of the reactant through this layer of product [61], as shown in Scheme 1c for a spherical particle. Among the expressions found in this group are the one-dimensional diffusion model for a flat plate [20] and the two-dimensional diffusion models for cylindrical [22] and cubic [23] particles. In the case of three-dimensional (3D) diffusion models for spherical particles, two expressions have been reported in the literature: the Jander equation [24], which assumes that the product layer thickness is related to reaction time by a parabolic rate law, and the Dunwald–Wagner equation [25], which is derived from Fick's second law of diffusion. Of these two expressions, the Jander model is the most representative. Indeed, numerous modifications of this model, including the Valensi–Carter [26,31], Serin–Ellickson [27], Zhuravlev–Lesokhin–Tempel'man [28], Ginstling–Brounshtein [29] and Kroger–Ziegler [30] models, have been reported.

These models have been widely applied in many gas–solid reactions. Similarly, in metal oxide reduction reactions, Tarfaoui [5] employed the Jander model in the reduction of copper, manganese and vanadium oxides, while other researchers have used this model to study the reduction of copper oxide [52], silver oxide [51] and iron oxide [9,14,54]. In the current study, the Jander (J) model was applied using Eq. (8):

$$\left[1-(1-\alpha)^{\frac{1}{3}}\right]^2=\frac{k\bullet t}{\left(\frac{d_p}{2}\right)^2} \tag{8}$$

where, in this case, the units for the reaction constant (k) are $m^2{\cdot}s^{-1}$. It can be seen from Eq. (8) that, unlike the geometrical contraction and nucleation models, the relationship with particle size (d_p) is quadratic in this type of model.

3.1.3. Nucleation models

Nucleation models are based on a two-stage reaction mechanism involving the initial formation of nuclei from seeds, as shown in Scheme 1b for a spherical particle, followed by the growth of these nuclei, which causes the reaction interface (reactant-product) to increase. Nuclei growth subsequently continues until the reactant is completely consumed [62]. In this sense, nucleation models are derived from expressions relating nucleation and nuclei growth rates to the kinetics of solid-state reactions, with the most representative mathematical equations being the Avrami model [32], which considers a single-stage nucleation, and the Prout and Tompkins model [33], which is based on a homogeneous reaction in which the product (nuclei formed) autocatalyzes the reaction of the remaining reactant. The former has been applied in the reduction of copper oxide [52], silver oxide [51], chromium oxide [10] and iron oxide [14,55], and the latter has been successfully employed in the reduction of copper oxide [5,7,11,52] and nickel oxide [11]. In the present study, the Prout and Tompkins (PT) equation was used as nucleation model, with the general form being as follows:

$$ln\left(\frac{\alpha}{1-\alpha}\right)=\frac{k\bullet t}{\left(\frac{d_p}{2}\right)}+C \tag{9}$$

where C is a constant of the PT model and the reaction constant (k) is in $m{\cdot}s^{-1}$.

3.2. Temperature dependence of the solid-state reaction kinetic models

In all expressions of solid-state reaction kinetic models (e.g., Eqs. (7)–(9)), it is necessary to know the reaction constant (or rate coefficient, k), which mainly depends on the reaction temperature (T). The most important quantitative relationship between them is the Arrhenius equation [63], which is based on the premise that, for a reaction to occur, an energy barrier must be overcome [19]. The Arrhenius temperature dependence of the rate constant is defined as follows:

$$k=A\bullet e^{\left[-\frac{E_a}{R\bullet T}\right]} \tag{10}$$

where A is the pre-exponential factor (in the same units as k), E_a is the energy activation (in $kJ{\cdot}mol^{-1}$), R is the universal gas constant (8.314×10^{-3} $kJ{\cdot}mol^{-1}{\cdot}K^{-1}$) and T is the absolute reaction temperature (in K).

TPR is an experimental technique, performed under non-isothermal conditions, in which a sample is heated at a constant rate (linearly), therefore the reaction temperature as a function of reaction time is given by Eq. (11):

$$\beta=\frac{dT}{dt} \tag{11}$$

where β is the linear heating rate (in $K{\cdot}s^{-1}$) and t is the reaction time (in s).

With regard to activation energy (E_a), this is the minimum energy that reactant molecules must acquire to react and can therefore be seen as a potential barrier that can provide information about the reaction mechanism. The most appropriate methodology for estimating the activation energy involves use of the Kissinger equation [64], which was derived for simple, thermally activated Arrhenian processes assuming that the conversion degree, which corresponds to the maximum reaction rate, is constant and does not depend on the experimental conditions [65]. The Kissinger expression is represented by Eq. (12):

$$ln\left(\frac{\beta}{T_P{}^2}\right)=-\frac{E_a}{R\bullet T_P}+B \tag{12}$$

where T_P is the absolute temperature corresponding to the position of the maximum peak signal, and B is a constant of the Kissinger equation. T_P values can be determined using non-isothermal measurement techniques such as TPR, DSC, DTA or DTG. Thus, based on Eq. (12), a plot of $ln\left(\frac{\beta}{T_P{}^2}\right)$ vs $\frac{1}{T_P}$ should be a straight line with a slope equal to $-\frac{E_a}{R}$.

3.3. Simulation of TPR patterns

3.3.1. Simulated individual TPR profiles

As mentioned above, the H_2-TPR technique can be used to obtain experimental data to generate the TCD signal vs T profile and reduction-temperature curve, which are related theoretically by means of Eq. (6) ($-\left(\frac{1}{V_p}\right)\frac{dV}{dt}$ vs T and α vs T, respectively). For this reason, Eq. (6) needs to be resolved in order to obtain the mathematical relationship between the reduction reaction rate (or degree of reaction) and the reaction temperature/time. The latter two are related to each other by the following expression (obtained from Eq. (11)):

$$T=T_0+\beta\bullet t \tag{13}$$

where the temperature T is a linear function of time:

As such, solving Eq. (6) employing Eq. (13) and Eqs. (7), (8) and (9) can give the exact analytical solution corresponding to each type of reaction model considered in this work, thus giving the following expressions:

For the CV model (geometrical contraction model):

$$-\left(\frac{1}{V_p}\right)\frac{dV}{dt}=\frac{6}{\left(\frac{d_p}{2}\right)^3}\bullet\left[\left(\frac{d_p}{2}\right)^2\bullet A\bullet e^{\left[-\frac{E_a}{R\bullet T}\right]}-4\bullet\left(\frac{d_p}{2}\right)\bullet A^2\bullet e^{\left[-\frac{2\bullet E_a}{R\bullet T}\right]}\bullet t+4\bullet A^3\bullet e^{\left[-\frac{3\bullet E_a}{R\bullet T}\right]}\bullet t^2\right]\bullet\left(1+\frac{E_a\bullet\beta}{R\bullet T^2}\bullet t\right) \tag{14}$$

For the J model (diffusion model):

$$-\left(\frac{1}{V_p}\right)\frac{dV}{dt}=\frac{3\bullet\left(2\bullet A\bullet e^{\left[-\frac{E_a}{R\bullet T}\right]}\right)^{\frac{1}{2}}}{2\bullet\left(\frac{d_p}{2}\right)^3\bullet t^{\frac{1}{2}}}\bullet\left[\left(\frac{d_p}{2}\right)-\left(2\bullet A\bullet e^{\left[-\frac{E_a}{R\bullet T}\right]}\bullet t\right)^{\frac{1}{2}}\right]^2\bullet\left(1+\frac{E_a\bullet\beta}{R\bullet T^2}\bullet t\right) \tag{15}$$

For the PT model (nucleation model):

$$-\left(\frac{1}{V_p}\right)\frac{dV}{dt}=A\bullet e^{\left[-\frac{E_a}{R\bullet T}\right]}\bullet\left[\frac{e^{\left[A\bullet e^{\left[-\frac{E_a}{R\bullet T}\right]}\bullet t+C\right]}}{\left(1+e^{\left[A\bullet e^{\left[-\frac{E_a}{R\bullet T}\right]}\bullet t+C\right]}\right)^2}\right]\bullet\left(1+\frac{E_a\bullet\beta}{R\bullet T^2}\bullet t\right) \tag{16}$$

Eqs. (14), (15) and (16) represent simulated individual TPR profiles for spherical particles of a given diameter d_p.

3.3.2. Modeling TPR profiles considering the PSD

An independent particle model was used to obtain the simulated H_2-TPR profile. This model assumes that all particles with various particle sizes are reduced independently from each other. Hence, considering the definition of *generalized adsorption isotherm* or *integral adsorption equation* [66], and relating it to TPR modeling, the experimental H_2-TPR profile for the metal oxide was described as a linear combination (or sum) of the TPR profiles for individual spherical particles. In mathematical terms, this can be written as:

$$g_{exp}(T)=\sum_{d_{p-min}}^{d_{p-max}}\left[g_{teo}(T,d_p)\bullet f_V(d_p)\right] \tag{17}$$

where $g_{exp}(T)$ represents the normalized experimental H_2-TPR data for the metal oxide, T is the temperature at time t, d_p is the particle size, $g_{teo}(T,d_p)$ is the normalized simulated TPR profile of an individual particle of size d_p, and $f_V(d_p)$ is the volume fraction of the particle of size d_p obtained from the PSD of the solid, which presents a minimum and a maximum particle size (d_{p-min} and d_{p-max}, respectively). The normalized experimental H_2-TPR data for the metal oxide ($g_{exp}(T)$) and the normalized simulated TPR profile of an individual particle ($g_{teo}(T,d_p)$) were obtained using Eqs. (18) and (19), respectively:

$$g_{exp}(T)=\frac{TCD_{signal}(T)}{\left(TCD_{signal}(T)\right)_{max}} \tag{18}$$

$$g_{teo}(T,d_p)=\frac{-\left(\frac{1}{V_p}\right)\frac{dV}{dt}\Big|_{T,d_p}}{\left(-\left(\frac{1}{V_p}\right)\frac{dV}{dt}\Big|_{T,d_p}\right)_{max}} \tag{19}$$

where $TCD_{signal}(T)$ is the experimental TCD signal at temperature T, $\left(TCD_{signal}(T)\right)_{max}$ is the maximum value of the experimental TCD signal, $-\left(\frac{1}{V_p}\right)\frac{dV}{dt}\Big|_{T,d_p}$ is the value of the simulated individual TPR profile corresponding to temperature T and particle size d_p (obtained using Eqs. (14), (15) or (16)), and $\left(-\left(\frac{1}{V_p}\right)\frac{dV}{dt}\Big|_{T,d_p}\right)_{max}$ is the maximum value of the $-\left(\frac{1}{V_p}\right)\frac{dV}{dt}\Big|_{T,d_p}$ data.

In order to determine the error of the fit (R_{ERROR}), the residual sum of least squares method was applied to the normalized experimental H_2-TPR data and the corresponding modeling output using Eq. (20):

$$R_{ERROR}=\sum_{T_0}^{T_F}\left[g_{exp}(T)-\sum_{d_{p-min}}^{d_{p-max}}\left[g_{teo}(T,d_p)\bullet f_V(d_p)\right]\right]^2 \tag{20}$$

where T_0 is the initial temperature of the TPR analysis and T_F is the final temperature at which the metal oxide reduction was complete. As such, the values of the pre-exponential factor (A) and/or energy activation (E_a) that minimize the R_{ERROR} parameter were obtained by selecting the type of reaction model and using Eq. (20) with twenty different particle size values (d_p) together with their corresponding volume fraction (according to the PSD).

All modeling calculations were performed in Microsoft Excel and the objective function R_{ERROR} (Eq. (20)) was minimized using the Solver add-in.

After determining the E_a value and the parameters of the best solid-state reaction kinetic model, Eq. (20) could be used to obtain the PSD that achieves the best fit of the normalized re-simulated TPR profile to the normalized experimental H_2-TPR data. However, the use of Eq. (20) leads to a noisy PSD (with many irregularities), which is why it is necessary to smooth the obtained PSD. For this purpose, various methods, known as regularization methods, have been proposed. One of the most widely used and accepted methods most in the field of adsorption was proposed by Davies et al. [67], which incorporates a term representing the smoothness of the PSD (R_{REG}) into the error of the fit (R_{ERROR}) to obtain the overall fitting error ($R_{OVERALL}$), as shown in Eq. (21):

$$R_{OVERALL}=R_{ERROR}+\mu\hat{A}\cdot R_{REG} \tag{21}$$

where μ (in μm^3) is the parameter (constant) that determines the weight of the roughness of the PSD in the overall fitting error and the R_{REG} (in μm^{-3}) is defined by Eq. (22):

$$R_{REG}=\sum_{d_{p-min}}^{d_{p-max}}\left[\left(f_V(d_p)^{(2)}\right)^2\bullet\delta d_p\right] \tag{22}$$

where the $f_V(d_p)^{(2)}$ term represents the roughness of the PSD, indicated by the second derivative of the volume fraction, $f_V(d_p)$, with respect to particle of size, d_p. This second derivative was evaluated using the approximation method of finite differences [67].

4. Results and discussion

Fig. 1 presents the powder XRD patterns of the metal oxides under study. All peaks found in these powder XRD patterns show the presence of a single-phase for CuO (PDF: 00–048-1548), Ag_2O (PDF: 00–012-0793), and NiO (PDF: 00–044-1159). The average crystallite sizes (D) were estimated by applying the Scherrer equation to the XRD data, specifically, the reflections used were: *i)* (1 1 1), (1 1—1), (2 0—2), and (1 1—3) for CuO, *ii)* (1 1 1), (2 0 0), and (2 2 0) for Ag_2O, and *iii)* (0 1 2), (1 0 1), and (1 1 0) for NiO. With these data, the D values of the metal oxides were (100 ± 12) nm, (45 ± 5) nm, and (25 ± 2) nm for CuO, Ag_2O, and NiO, respectively.

The PSD histograms for the CuO, Ag_2O and NiO powders obtained from SEM micrographs are presented in Fig. 2**a, 2b and 2c**, respectively. As seen in this figure (insets): *i)* CuO powder consists of an aggregate of

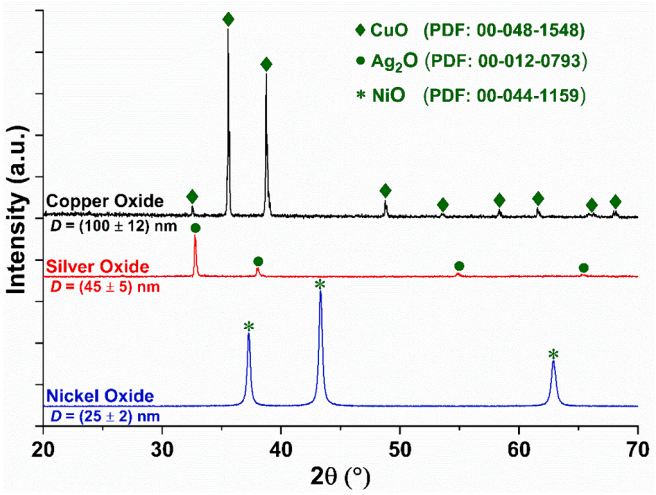

Fig. 1. XRD patterns for CuO, Ag_2O, and NiO.

particles with varied sizes and shapes; *ii)* Ag_2O powder presents particles with a spherical-like shape and a more homogeneous size; and, *iii)* NiO powder exhibits an aggregate of particles with irregular shapes but smaller sizes. The SEM images also show a unimodal PSD with a modal particle size, based on the number of particles, of 1.7, 1.1 and 0.048 μm for CuO, Ag_2O, and NiO, respectively. However, the PSD of the CuO sample also exhibits another group of particle sizes (a shoulder) of approximately 3.2 μm. The particle size measurements by SEM images have an approximate error equivalent to 1 pixel of the micrograph, which is 0.06 μm for CuO, 0.02 μm for Ag_2O and 0.002 μm for NiO. Furthermore, it is also important to mention that if the PSD is based on the volume of the particles, a modal particle size of 5.1, 1.3 and 0.065 μm was found, respectively. The difference between these modal particle sizes (based on the number of particles vs based on the volume of the particles) is due to the fact that the one obtained by the distribution based on the number of particles has the characteristic that each particle has equal weight, regardless of its size. Meanwhile, the one obtained from a distribution based on the volume of particles has the characteristic that the size of each particle is weighted by its volume. Between these two types of distributions, the one based on the volume of particles is the most suitable for correlating with catalytic performance. For this reason, it is the distribution considered in the mathematical modeling (Eq. (17)). On the other hand, the modal particle sizes obtained are higher than the actual sizes of the crystallites, most likely due to the fact that each particle is made up of several such crystallites.

Regarding the particle shape distribution of the metal oxides, in Fig. 2**d**, it can be observed, in terms of circularity value, that the CuO and NiO samples exhibit a broad distribution of shapes ranging from 0.64 to 0.96 in circularity value, with a modal value of 0.91. In contrast, the Ag_2O sample shows a narrow distribution (between 0.89 and 0.975 in circularity value) with a modal value of 0.95. This indicates that this metal oxide has particles with more homogeneous sizes and more circular shapes, inferring that the particles are more spherical.

The experimental H_2-TPR patterns for the metal oxides at various nominal β values are displayed in Fig. 3. All profiles show only one peak, with the maximum reduction rate occurring at a specific temperature that depends on the β value in the ranges 590–650, 435–463, and 624–677 K, for CuO, Ag_2O, and NiO, respectively. These results indicate that the reduction of these metal oxides occurs in a single step, i.e., CuO to Cu^0, Ag_2O to Ag^0 and NiO to Ni^0. Although it has been reported that the H_2 reduction of CuO and NiO may occur in a single step in terms of H_2 consumption, the reduction process may not be a single step, and there may also be an induction time with an autocatalytic stage [68–70]. The H_2-TPR patterns for NiO have the highest reduction temperatures and broadest peaks, while those for Ag_2O show the opposite trend. The behavior of the H_2 reduction process observed with different metal oxides, in terms of reduction temperature and peak width, provides crucial information about the catalytic properties and reactivity of these metal

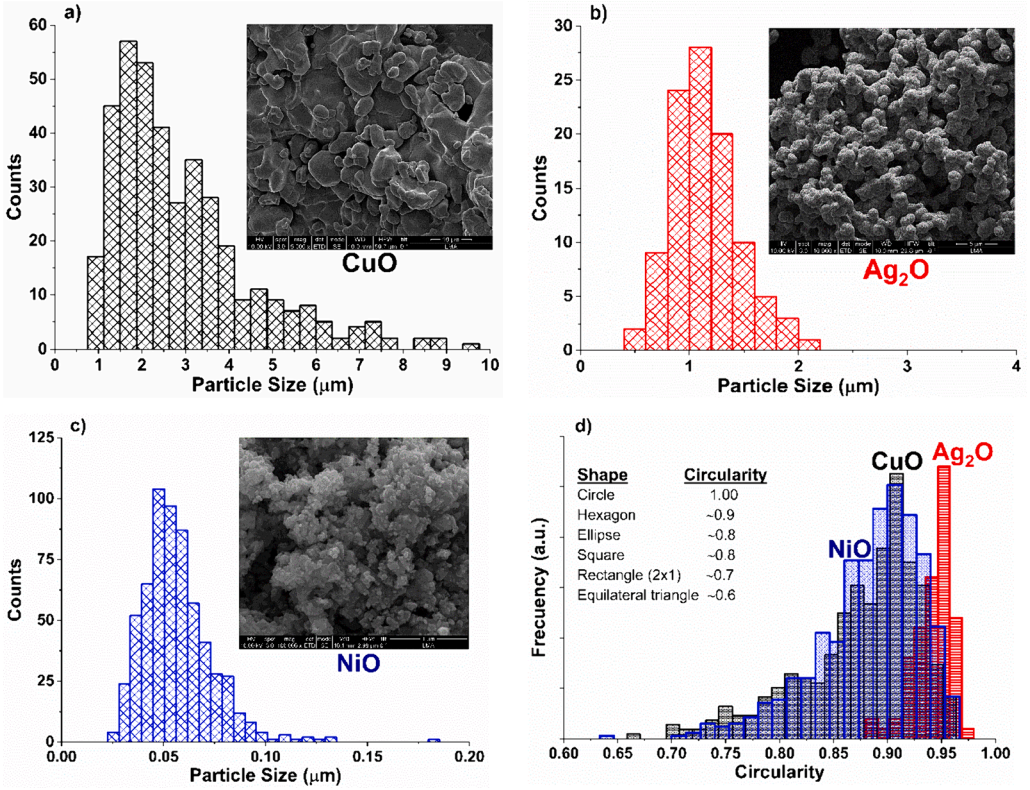

Fig. 2. PSD histograms and the corresponding SEM micrographs for a) CuO, b) Ag_2O, and c) NiO; and their d) distribution of particle shapes.

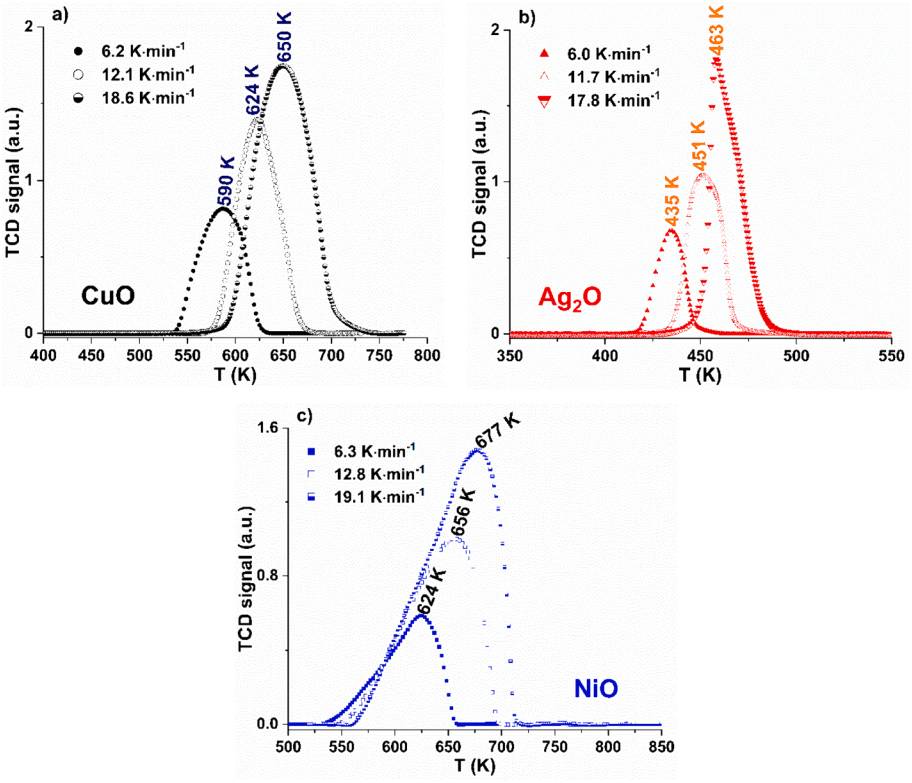

Fig. 3. Experimental H_2-TPR patterns at various nominal heating rates (6, 12, and 18 K·min^{-1}) for: a) CuO, b) Ag_2O, and c) NiO. Each H_2-TPR pattern was obtained with a fresh sample.

oxides. Specifically, by comparing reduction temperatures, it indicates the ease with which each metal oxide releases oxygen and undergoes reduction in the presence of hydrogen, while differences in peak widths indicate the relative quantity of active sites present in the catalyst. In this work, this latter behavior is directly associated with the PSD.

Plots of $ln\left(\frac{\beta}{T_P^2}\right)$ vs $\frac{1}{T_P}$ were obtained using the maximum reduction rate temperatures (T_P) from the experimental H_2-TPR patterns of the corresponding metal oxides at various β values by applying the Kissinger method (Eq. (12)), as shown in Fig. 4. These plots show good straight lines with correlation coefficients (R^2) of more than 0.998. The slopes of these straight lines give reduction activation energy (E_a) values of 48.7, 59.0, and 62.8 kJ·mol^{-1} for CuO, Ag_2O, and NiO, respectively.

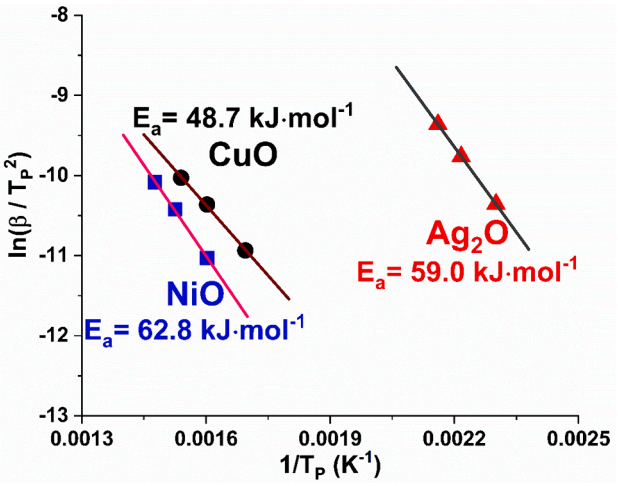

Fig. 4. Kissinger plots of the experimental H_2-TPR patterns for CuO, Ag_2O, and NiO powders.

Table 1 compares the calculated reduction activation energy values for the metal oxides studied with those found in the recent literature obtained using the Kissinger method or the Friedman method [71], which considers the degree of reduction (α). Our values fall within the range of reported values, with a reasonable agreement between them. However, some reported activation energy values are rather high, which could be attributed to the effect of the particle size difference.

Fig. 5 shows an example of a set of simulated individual TPR profiles for the reduction of various NiO particle sizes, which was obtained using the PT model (Eqs. (13) and (16)) with defined model parameters (E_a, A and C values) and experimental conditions (T_0 and β values). As expected, these profiles show that the temperature at which reduction occurs increases with particle size [6,37]. This is because, at the reaction interface of the smaller particles, metallic nuclei form more rapidly through the growth of already formed nuclei and those that are being formed, until these nuclei start to come into contact with each other. This causes the oxide to be completely reduced to metal at a temperature lower than that which would occur in larger particles [1]. The particle sizes values selected to generate the profiles in Fig. 5 were chosen based on the PSD of the NiO sample (Fig. 2**c**), which presents particle sizes ranging between 0.025 and 0.132 μm. Thus, it is possible to perform a linear combination of these simulated individual TPR profiles with the volume fractions corresponding to each particle size to obtain a global simulated H_2-TPR profile that best fits the experimental H_2-TPR pattern (using Eq. (20)).

A fit of the global simulated H_2-TPR profile with the experimental H_2-TPR pattern performed considering a single heating rate value gave simulated H_2-TPR patterns for the metal oxides under study with several solid-state kinetic models, as shown in Fig. 6. The results show that, when the E_a value obtained using the Kissinger method is used (48.7, 59.0, and 62.8 kJ·mol^{-1}, for CuO, Ag_2O, and NiO, respectively), the simulated profiles obtained using the CV and J models do not fit well with the experimental H_2-TPR profiles. However, if both models are applied using another E_a value in order to fit the simulated profile to the

Table 1
Comparison of the calculated E_a values with those reported in the literature for metal oxides.

Metal Oxide	Solid	E_a (kJ·mol^{-1})	Model/Method	Reference
Copper oxide	CuO	44.0	Friedman	[5]
	CuO	45.0	Kissinger	[11]
	CuO	48.7	Kissinger	This work
	CuO	53.0	Kissinger	[5]
	CuO	60.2/64.9	Kissinger	[7]
	CuO	38.0	Prout and Tompkins	[11]
	CuO	47.7	Prout and Tompkins	This work
	CuO	51.2	Avrami	[5]
	CuO	60.5/65.6	Prout and Tompkins	[7]
Silver oxide	Ag_2O	59.0	Kissinger	This work
	Ag_2O	59.7	Kissinger	[75]
	Ag/TiO_2	73.4/81.7	Kissinger	[51]
	Ag_2O	52.6	Prout and Tompkins	This work
	Ag_2O/MoO_3	64.0	Contracting Volume	[76]
Nickel oxide	NiO/YSZ	54.0/77.0	Friedman	[77]
	NiO	62.8	Kissinger	This work
	NiO	63.7	Friedman	[78]
	NiO	68.0	Kissinger	[79]
	NiO	69.0	Kissinger	[11]
	NiO	82.0	Third-law	[80]
	NiO	85.0	Kissinger	[81]
	NiO	85.6	Friedman	[82]
	NiO	90.8	Friedman	[56]
	NiO	91.8/94.5	Friedman	[83]
	NiO/Al_2O_3	95.0	Kissinger	[84]
	NiO	98.4	Kissinger	[57]
	NiO	54.0	Prout and Tompkins	[11]
	NiO	70.5	Prout and Tompkins	This work
	NiO	84.0/109	Avrami	[85]
	NiO	90.0	Contracting Volume	[86]
	NiO	107	Avrami	[87]

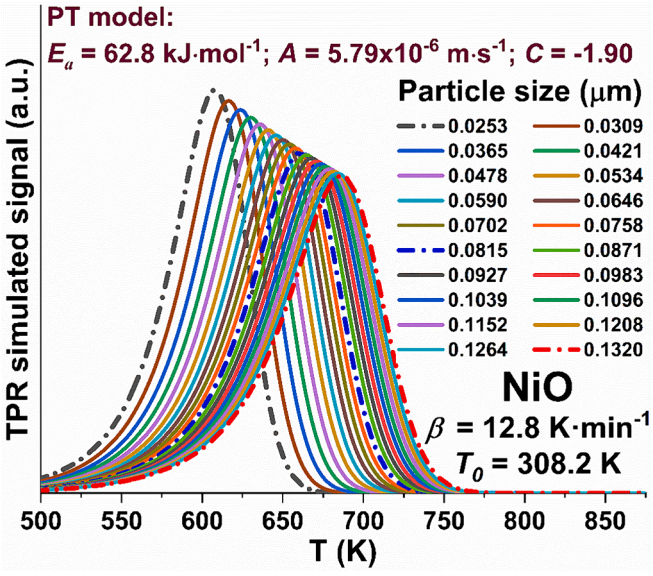

Fig. 5. Set of simulated individual TPR profiles for NiO particles of several diameters (d_p) using the PT model for a β value of 12.8 K·min^{-1}.

experimental data, values of 96–193 and 199–318 kJ·mol^{-1}, respectively, are obtained. These high E_a values mean that the simulated profiles only fit the experimental data for a heating rate (e.g., 6.2 K·min^{-1} for CuO), and not for the other conditions (e.g., 18 K·min^{-1} for CuO). These results indicate that the kinetic reduction of these metal oxides is not governed by the geometrical contraction and diffusion models. Furthermore, these results show that, in the modeling of H_2-TPR profiles, the correct choice of the reaction kinetic model is crucial. Depending on the kinetic model used, either broader profiles than the experimental ones will be obtained, or high activation energy values will be obtained, which do not correspond to those obtained with other techniques/models. Fig. 6 also shows that, using the PT model (with E_a values obtained using the Kissinger method), a good agreement between the simulated profile and the experimental H_2-TPR pattern was obtained. This result suggests that the kinetic reduction of CuO, Ag_2O, and NiO powders, under non-isothermal conditions, obeys a nucleation mechanism, thereby suggesting that the reduction of Cu^{2+}, Ag^{+}, and Ni^{2+} to Cu^0, Ag^0, and Ni^0, respectively, takes place randomly on the surface of the solid in any available space containing a reducible metal. This result is in agreement with what has been reported by Jeangros et al. [72], which, to our knowledge, is the only experimental evidence. They examined a sample of NiO in an environmental transmission electron microscope in an H_2 atmosphere, through which they could observe the formation and growth of nuclei (important in the nucleation mechanism).

Finally, in order to show the effect of PSD on the simulated H_2-TPR pattern, Fig. 6 also includes the simulated H_2-TPR profile of an individual particle size (corresponding to a modal particle size when the PSD is based on the volume of the particles) of 5.1, 1.3, and 0.065 μm, for CuO, Ag_2O, and NiO, respectively. A clear difference can be observed in all cases since the profile shown is narrower than the experimental one, thus indicating the missing contribution from smaller and larger particles.

The parameter values of the solid-state kinetic models obtained by fitting the global simulated H_2-TPR profile with the experimental H_2-TPR pattern, considering a single heating rate value, are shown in Table 2. This table presents two E_a values for the CV and J models, with the lowest values being obtained using the Kissinger method, whereas the highest values are those obtained to achieve the best fit of the simulated H_2-TPR profile to the experimental H_2-TPR pattern. In addition, the results shown in Table 2 reflect the previous discussion, whereby, unlike the other kinetic models, the correlation coefficient (R^2) for the PT model gives values between 0.959 and 0.993.

The profiles shown in Fig. 7 are obtained by performing a simultaneous fit of the global simulated H_2-TPR profiles (using the PT model) for the three heating rate values to their corresponding experimental H_2-TPR patterns (varying the E_a, A and C values). The degree of reduction curves presented in Fig. 8 were obtained from those profiles. These two figures reveal that the simulated profiles/curves are in very good agreement with the experimental data. This means that the PT model gives a good description of the reduction of CuO, Ag_2O, and NiO, and confirms that the reduction process is governed by a nucleation mechanism. The values of the PT model parameters for the metal oxides under study are shown in Table 3.

The new E_a values obtained are also summarized in Table 3 and are in good agreement with those estimated using the Kissinger method. This indicates that the Kissinger method gives results with a very good approximation. It is important to highlight that the E_a value depends on many factors [1,15,73], such as: *i)* particle size of the metal oxide, *ii)* temperature and pressure of H_2 during reduction, *iii)* chemical nature of the metal oxide, and *iv)* initial oxidation state of the metal oxide. Therefore, it is crucial that the present modeling proposal be conducted using data obtained under the same experimental conditions, with the only variation between each experiment being the heating rate (β). A comparison of the E_a values obtained (using the PT model; see Table 3) with those reported in the literature (using various kinetic models; see

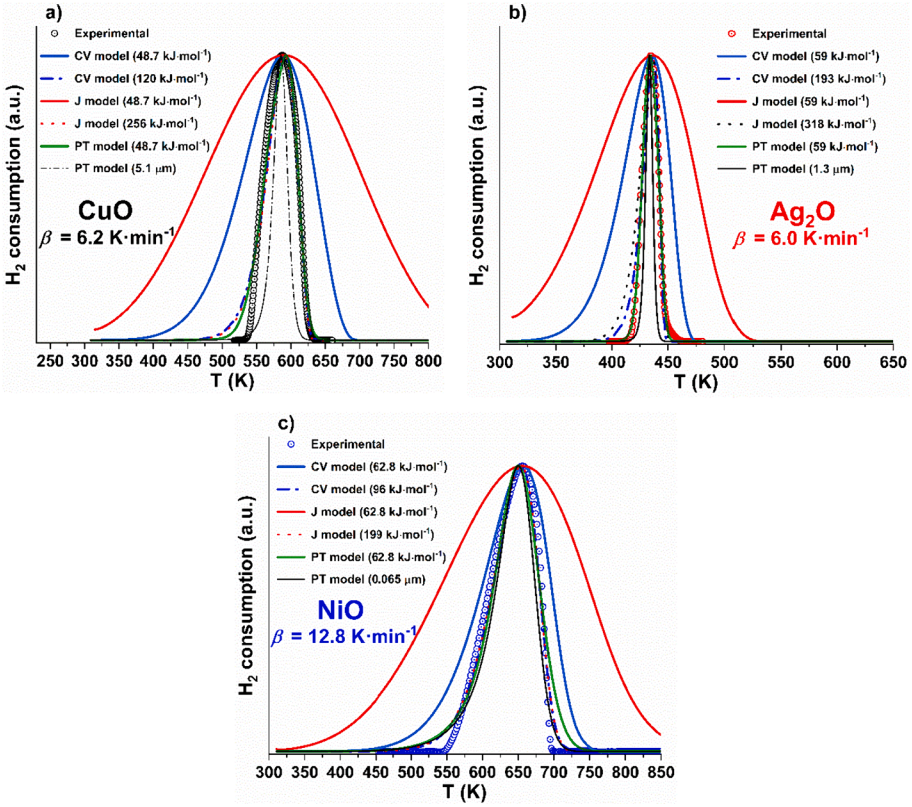

Fig. 6. Experimental and simulated H_2-TPR patterns for: a) CuO (β=6.2 K·min^{-1}), b) Ag_2O (β=6.0 K·min^{-1}), and c) NiO (β=12.8 K·min^{-1}).

Table 2
Values for the kinetic model parameters of the global simulated H_2-TPR profiles for CuO, Ag_2O, and NiO obtained considering the profile of a single β value.

Metal Oxide	Model	E_a (kJ·mol^{-1})	A (m·s^{-1} or m^2·s^{-1})*	C	R^2
CuO	**CV**	48.7	4.90x10^{-6}	–	−0.105
T_o = 307.6		120	1.07x10^{1}	–	0.962
K	**J**	48.7	1.00x10^{-12}	–	−1.689
β = 6.2		256	3.67x10^{6}	–	0.962
K·min^{-1}	**PT**	48.7	1.51x10^{-4}	−6.99	0.975
Ag_2O	**CV**	59.0	1.80x10^{-3}	–	−0.919
T_o = 305.4		193	2.16 x10^{13}	–	0.967
K	**J**	59.0	1.40x10^{-10}	–	−4.186
β = 6.0		318	2.40x10^{21}	–	0.902
K·min^{-1}	**PT**	59.0	7.25x10^{-2}	−10.87	0.993
NiO	**CV**	62.8	5.80x10^{-7}	–	0.791
T_o = 308.2		95.7	2.72x10^{-4}	–	0.989
K	**J**	62.8	2.10x10^{-15}	–	−0.486
β = 12.8		199	2.40x10^{-4}	–	0.989
K·min^{-1}	**PT**	62.8	5.79x10^{-6}	−1.90	0.959

* m·s^{-1} for CV and PT models, and m^2·s^{-1} for J model.

Table 1) shows that there is a reasonable agreement between them. However, in the case of the reduction of CuO and NiO, some of the E_a values are higher than those obtained, which, as mentioned above, may be associated with the effect of the difference in particle size of the samples analyzed. The results included in Table 3 also show that a global correlation coefficient (R^2) of more than 0.951 is obtained when using the PT model, where the Ag_2O sample exhibits the best fit (R^2 = 0.97). This could be related to the fact that, as mentioned before, this metal oxide displayed more spherical particles.

With the values of the PT model parameters already determined for each metal oxide (Table 3), a re-simulation of the modeling was performed (using Eq. (21)) to obtain a new particle size distribution whose global simulated H_2-TPR profile better fits the experimental H_2-TPR pattern. In this regard, improved fits were achieved, as can be observed in Fig. 5S and 6S, attaining values of the global correlation coefficients (Table 1S) higher than 0.961. In Table 1S, the values of the μ parameter and the corresponding errors (R_{ERROR} and $R_{OVERALL}$) obtained in the re-simulation are also presented.

The comparison of particle size distributions (experimental and that obtained by the re-simulation of the modeling) presented in Fig. 9 shows that: *i)* in the case of Ag_2O, both PSDs are very similar, with both having a modal particle size of 1.1 μm; *ii)* in the case of NiO, although both PSDs present a very similar shape for the distribution profile, the peak for the new PSD obtained changes slightly toward a smaller value (from 0.048 to 0.042 μm); and *iii)* in the case of CuO, unlike the PSD obtained from SEM images (which shows its main distribution at a modal size of 1.7 μm and a shoulder at 3.2 μm), the new PSD exhibits a clear unimodal distribution with a modal size coinciding with of the shoulder in the experimental PSD. Although the experimental PSDs of all metal oxides were obtained using several SEM images and taking several particles in each of them, small differences are observed between both PSDs (experimental and re-simulation of the modeling). These results can be explained by the fact that the PSD values obtained from the SEM images depend on several factors, such as: *i)* the quality of the SEM images; *ii)* the fact that the SEM images represent a small portion of the sample, in other words they are not a global measurement; and, *iii)* the parameters required by the software to perform the image analysis [74]. Additionally, obtaining a PSD from SEM images is not trivial due to particle overlap. There are other methods of PSD analysis, with dynamic light scattering (DLS) being one of the most prominent. However, it is difficult to accurately assess the PSD due to the adhesion of individual particles, leading to the formation of aggregates. Therefore, with the DLS experimental technique, the size of these aggregates is measured, and not the individual size of the particles. In this sense, it is important to highlight the results obtained here given that, by using experimental data for the reduction of metal oxides using hydrogen as probe molecule, and employing mathematical modeling of H_2-TPR profiles, a PSD of the

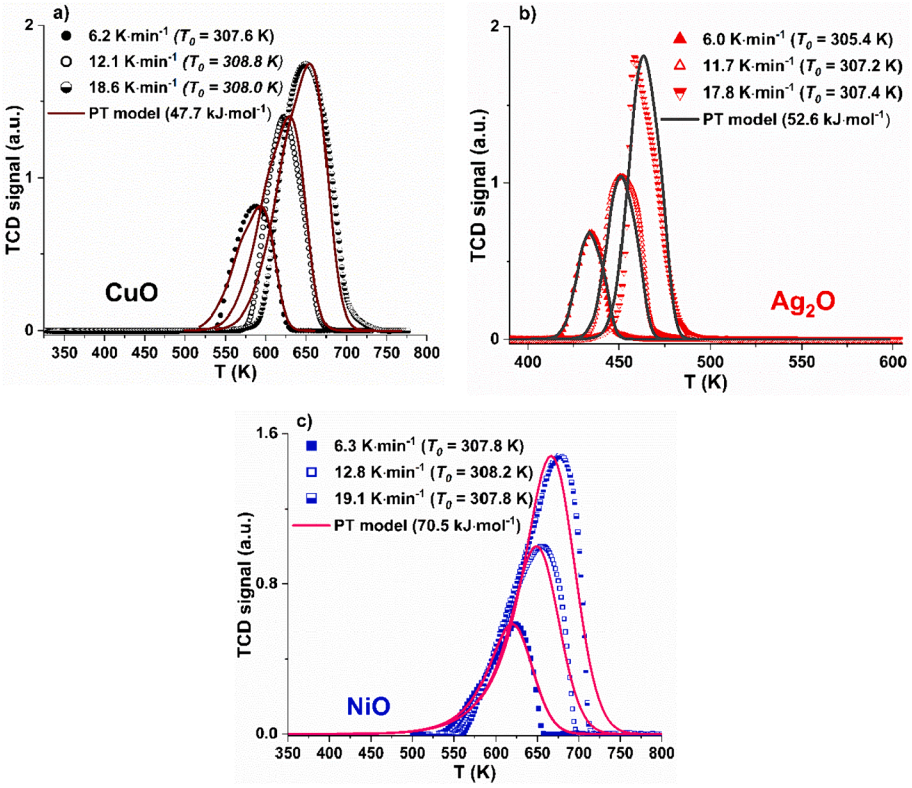

Fig. 7. Experimental (symbols) and simulated (lines) H_2-TPR profiles corresponding to the reduction of: a) CuO, b) Ag_2O, and c) NiO powders at various heating rates.

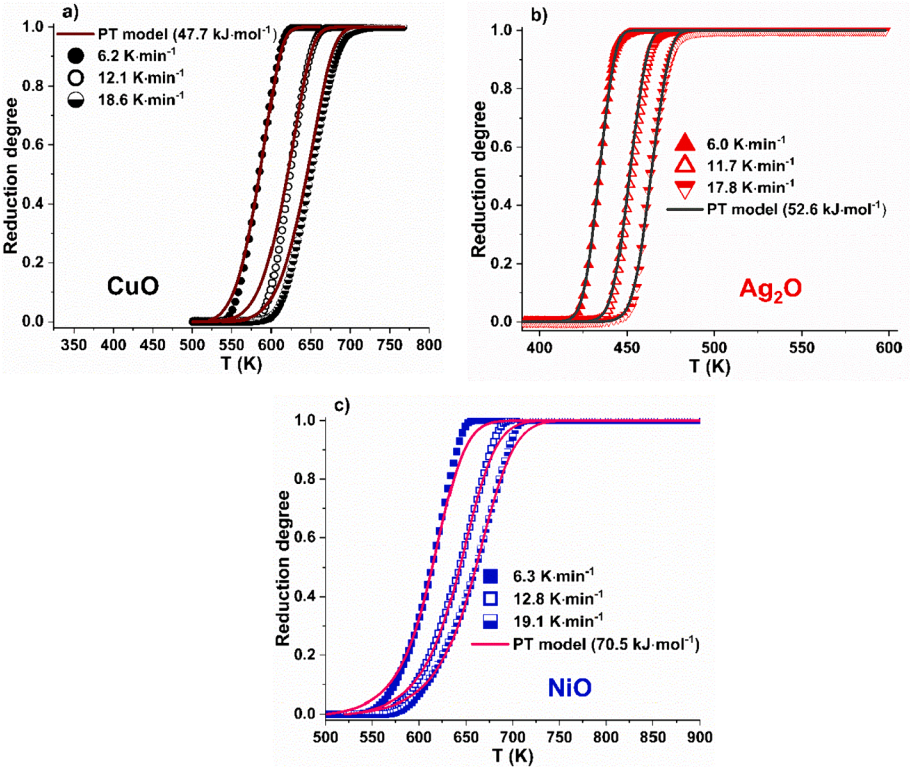

Fig. 8. Experimental (symbols) and simulated (lines) plots of degree of reduction (α) vs reaction temperature (T) corresponding to the reduction of: a) CuO, b) Ag_2O, and c) NiO powders at several heating rates.

Table 3
Values for the PT model parameters of the global simulated H_2-TPR profiles for CuO, Ag_2O, and NiO powders.

Metal Oxide	E_a (kJ·mol^{-1})	A (m·s^{-1})	C	R^2			
				β (K·min^{-1})			Global
				6*	12*	18*	
CuO	47.7	1.26x10^{-4}	−7.33	0.973	0.918	0.960	0.951
Ag_2O	52.6	1.54 x10^{-2}	−13.59	0.987	0.973	0.940	0.970
NiO	70.5	2.34x10^{-5}	− 1.68	0.957	0.961	0.951	0.956

* Nominal heating rate values.

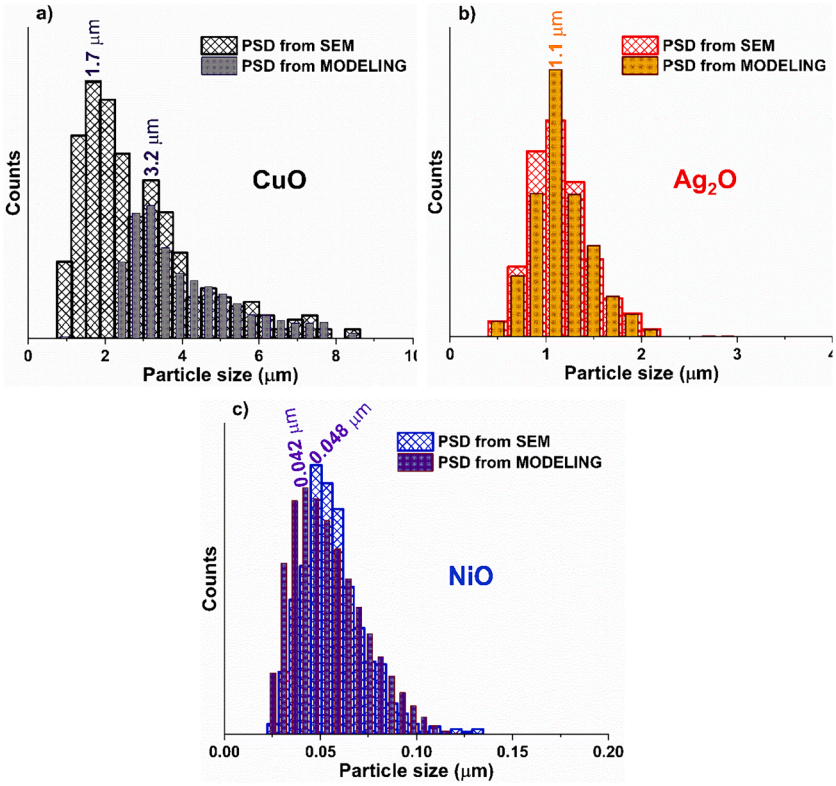

Fig. 9. PSDs obtained from SEM images and from modeling for: a) CuO, b) Ag_2O, and c) NiO.

metal oxide catalysts can be obtained that could better explain some results obtained in specific cases, for example, in the catalytic performance of environmental and energy applications involving gas–solid chemical reactions.

5. Conclusions

This work has measured H_2-TPR patterns for various metal oxides and has modeled these profiles considering the PSD effect.

The shape of the reduction curve (TPR) and at what temperatures the reaction occurs is a first criterion to establish whether there is interaction between the metal oxide particles and the surface of the support. If there is no clear difference between the TPR of the unsupported and supported metal oxide, it can be said that there are metal oxide particles without interacting with the support. Semiquantitatively, if the results of PSD obtained from modeling are significantly different from those obtained with the PSD estimated from SEM images, for example, by one or more orders of magnitude, this would indicate that the chemistry of the reduction of the studied metal oxides also depends not only on particle size but also on the support material interaction and/or confinement in the porous structure. In this case, the current modeling approach would be oversimplified, and the results obtained would not be satisfactory.

The results of modeling of H_2-TPR profiles using several solid-state reaction kinetic models showed that only with the Prout and Tompkins model were a good agreement between the simulated profile and the experimental H_2-TPR pattern was achieved (with correlation coefficients higher than 0.96, reaching values as high as 0.99 when the particles are spherical), and it also estimated activation energy values (47.7, 52.6 and 70.5 kJ·mol^{-1}, for CuO, Ag_2O and NiO, respectively) very consistent with those obtained using the Kissinger method and reported in the literature. In this regard, it can be concluded that: *i)* reduction of the metal oxides studied (CuO, Ag_2O, and NiO) is governed by a nucleation mechanism, i.e., the reduction process takes place randomly on the surface of the solid in any available space containing a reducible metal, and *ii)* the PSD of the metal oxide has an important effect on the resulting H_2-TPR profile, for example, if the PSD exhibits a wide distribution, the H_2-TPR profile will also show a broader reduction peak.

A simple procedure to model the TPR profile of metal oxides using the Prout and Tompkins model taking the PSD of the metal oxide into consideration is also described. These results suggest that modeling the experimental H_2-TPR profiles using a nucleation model can provide information regarding the PSD of metal oxide catalysts that present a single-step H_2 consumption in the reduction process and in which only the particle size difference effect is present.

Finally, the notable changes in the physical and chemical properties of metal oxide catalysts based on particle size emphasize the critical

importance of characterizing and controlling particle size distribution. Smaller particles are consumed in a shorter period than their larger counterparts, impacting the reaction rate per unit area or volume, which is dependent on the diameter of an individual particle. This consideration becomes especially relevant in catalyst design, particularly in fields like heterogeneous catalysis (e.g., in the context of energy-related research), with the fundamental goal of enhancing the selectivity, reactivity, and stability of these catalysts.

CRediT authorship contribution statement

Jhonny Villarroel-Rocha: Writing – review & editing, Writing – original draft, Methodology, Investigation, Formal analysis, Conceptualization. **Antonio Gil:** Writing – review & editing, Writing – original draft, Validation, Supervision, Resources, Methodology, Funding acquisition, Formal analysis, Conceptualization.

Declaration of competing interest

The authors declare that they have no known competing financial interests or personal relationships that could have appeared to influence the work reported in this paper.

Data availability

No data was used for the research described in the article.

Acknowledgment

The authors are grateful for the financial support received from the Spanish Ministry of Science and Innovation (MCIN/AEI/10.13039/501100011033) through project PID2020-112656RB-C21. Open access funding provided by Universidad Pública de Navarra. JVR thanks the Universidad Pública de Navarra for a post-doctoral María Zambrano grant, financed by the European Union-Next Generation EU.

Appendix A. Supplementary data

Supplementary data to this article can be found online at https://doi.org/10.1016/j.cej.2024.150722.

References

[1] A. Jones, B.D. McNicol, Temperature-programmed reduction for solid materials characterization, 1st ed., CRC Press, Boca Raton, 1986.
[2] A. Savara, Simulation and fitting of complex reaction network TPR: the key is the objective function, Surf. Sci. 653 (2016) 169–180.
[3] B. Pomeroy, M. Grilc, S. Gyergyek, B. Likozar, Catalyst structure-based hydroxymethylfurfural (HMF) hydrogenation mechanisms, activity and selectivity over ni, Chem. Eng. J. 412 (2021) 127553.
[4] R. Šivec, M. Huš, B. Likozar, M. Grilc, Furfural hydrogenation over cu, ni, pd, pt, re, rh and ru catalysts: ab initio modelling of adsorption, desorption and reaction micro-kinetics, Chem. Eng. J. 436 (2022) 135070.
[5] A. Tarfaoui, Modelling the kinetics on reduction by temperature programming, Delft University Press, 1996.
[6] K.H. Tonge, Particle size effects in temperature programmed topochemical reactions, Thermochim. Acta 74 (1984) 151–166.
[7] D. Jelić, B. Tomić-Tucaković, S. Mentus, A kinetic study of copper(II) oxide powder reduction with hydrogen, based on thermogravimetry, Thermochim. Acta 521 (2011) 211–217.
[8] F. Giordano, A. Trovarelli, C. De Leitenburg, M. Giona, A model for the temperature-programmed reduction of low and high surface area ceria, J. Catal. 193 (2000) 273–282.
[9] O.J. Wimmers, P. Arnoldy, J.A. Moulijn, Determination of the reduction mechanism by temperature-programmed reduction: application to small Fe_2O_3 particles, J. Phys. Chem. 90 (1986) 1331–1337.
[10] J.M. Kanervo, A.O.I. Krause, Characterisation of supported chromium oxide catalysts by kinetic analysis of H_2-TPR data, J. Catal. 207 (2002) 57–65.
[11] A.V. Fedorov, R.G. Kukushkin, P.M. Yeletsky, O.A. Bulavchenko, Y.A. Chesalov, V. A. Yakovlev, Temperature-programmed reduction of model CuO, NiO and mixed CuO–NiO catalysts with hydrogen, J. Alloys Compd. 844 (2020) 156135.
[12] D.A.M. Monti, A. Baiker, Temperature-programmed reduction. Parametric sensitivity and estimation of kinetic parameters, J. Catal. 83 (1983) 323–335.
[13] N.W. Hurst, S.J. Gentry, A. Jones, Temperature programmed reduction, Catal. Rev. 24 (1982) 233–309.
[14] P. Heidebrecht, V. Galvita, K. Sundmacher, An alternative method for parameter identification from temperature programmed reduction (TPR) data, Chem. Eng. Sci. 63 (2008) 4776–4788.
[15] M.J. Tiernan, P.A. Barnes, G.M.B. Parkes, New approach to the investigation of mechanisms and apparent activation energies for the reduction of metal oxides using constant reaction rate temperature-programmed reduction, J. Phys. Chem. B 103 (1999) 338–345.
[16] J.J. Torrez-Herrera, S.A. Korili, A. Gil, Structure and activity of nickel supported on hibonite-type la-hexaaluminates synthesized from aluminum saline slags for the dry reforming of methane, Chem. Eng. J. Adv. 5 (2021) 100080.
[17] I. Pedroarena, L. Grande, J.J. Torrez-Herrera, S.A. Korili, A. Gil, Analysis by temperature-programmed reduction of the catalytic system ni-mo-Pd/Al_2O_3, Fuel 334 (2023) 126789.
[18] W. Paul A., O. Clyde, C. Ronnie W., O. James P., Y.Y. Simon, Analytical Methods in Fine Particle Technology, 1st Edition, Micromeritics Instrument Corporation, 1997.
[19] A. Ortega, The kinetics of solid-state reactions toward consensus - Part I: uncertainties, failures, and successes of conventional methods, Int. J. Chem. Kinet. 33 (2001) 343–353.
[20] J.H. Sharp, G.W. Brindley, B.N. Narahari Achar, Numerical data for some commonly used solid state reaction equations, J. Am. Ceram. Soc. 49 (1966) 379–382.
[21] K.J. Laidler, Chemical kinetics, 2nd ed., McGraw-Hill, New York, 1965.
[22] J.B. Holt, I.B. Cutler, M.E. Wadsworth, Rate of thermal dehydration of kaolinite in vacuum, J. Am. Ceram. Soc. 45 (1962) 133–136.
[23] J. Jach, The thermal decomposition of NaBr O3 part I—Unirradiated material, J. Phys. Chem. Solids 24 (1963) 63–73.
[24] V.W. Jander, Reaktionen im festen zustande bei höheren temperaturen. reaktionsgeschwindigkeiten endotherm verlaufender umsetzungen, Z, Anorg. Allg. Chem. 163 (1927) 1–30.
[25] H. Dunwald, C. Wagner, Measurement of diffusion rate in the process of dissolving gases in solid phases, Z. Phys. Chem. (leipzig) B 24 (1934) 53–58.
[26] G. Valensi, Cinétique de l'oxydation de sphérules et de poudres métalliques, Compt. Rend. Acad. Sci. 202 (1936) 309–312.
[27] B. Serin, R.T. Ellickson, Determination of diffusion coefficients, J. Chem. Phys. 9 (1941) 742–747.
[28] V.F. Zhuravlev, I.G. Lesokhin, R.G. Tempel'man, Kinetics of the reactions for the formation of aluminates and the role of mineralizers in the process, Russ. J. Appl. Chem. 21 (1948) 887–902.
[29] A.M. Ginstling, B.I. Brounshtein, Concerning the diffusion kinetics of reactions in spherical particles, Russ. J. Appl. Chem. 23 (1950) 1327–1338.
[30] C. Kroger, G. Ziegler, Reaction rates of glass batch melting. III, reaction rates in the quaternary system Na_2O-CaO-SiO_2-CO_2, Glastech. Ber. 27 (1954) 199–212.
[31] R.E. Carter, Kinetic model for solid-state reactions, J. Chem. Phys. 34 (1961) 2010–2015.
[32] M. Avrami, Kinetics of phase change. II transformation-time relations for random distribution of nuclei, J. Chem. Phys. 8 (1940) 212–224.
[33] E.G. Prout, F.C. Tompkins, The thermal decomposition of potassium permanganate, Trans. Faraday Soc. 40 (1944) 488–498.
[34] S. Miyagi, A criticism on jander's equation of reaction-rate, considering the statistical distribution of particle size of reacting substance, J. Ceram. Soc. Jpn. 59 (1951) 132–135.
[35] H. Sasaki, Introduction of particle-size distribution into kinetics of solid-state reaction, J. Am. Ceram. Soc. 47 (1964) 512–516.
[36] K.J. Gallagher, The effect of particle size distribution on the kinetics of diffusion reactions in powders, in: G.M. Schwab (Ed.), Reactivity of Solids, Elsevier, New York, 1965, pp. 192–203.
[37] J. Arcenegui-Troya, P.E. Sánchez-Jiménez, A. Perejón, L.A. Pérez-Maqueda, Relevance of particle size distribution to kinetic analysis: the case of thermal dehydroxylation of kaolinite, Processes 9 (2021) 1852.
[38] J. Cho, H.Y. Sohn, Effects of particle shape and size distribution on the overall fluid-solid reaction rates of particle assemblages, Can. J. Chem. Eng. 94 (2016) 1516–1523.
[39] H.G. Mcllvried, F.E. Massoth, Effect of particle size distribution on gas-solid reaction kinetics for spherical particles, Ind. Eng. Chem. Fun. 12 (1973) 225–229.
[40] R.B. Anderson, J. Bayer, L.J.E. Hofer, Linear solutions of Fick's law, Ind. Eng. Chem. Process Des. Dev. 4 (1965) 167–171.
[41] D.M. Ruthven, K.F. Loughlin, The effect of crystallite shape and size distribution on diffusion measurements in molecular sieves, Chem. Eng. Sci. 26 (1971) 577–584.
[42] P.W. Brown, Effects of particle size distribution on the kinetics of hydration of tricalcium silicate, J. Am. Ceram. Soc. 72 (1989) 1829–1832.
[43] E.A. Cooper, T.O. Mason, Mechanism of La_2CuO_4 solid-state powder reaction by quantitative XRD and impedance spectroscopy, J. Am. Ceram. Soc. 78 (1995) 857–864.
[44] P.C. Kapur, Kinetics of solid-state reactions of particulate ensembles with size distributions, J. Am. Ceram. Soc. 56 (1973) 79–81.
[45] G.A. Urrutia, M.A. Blesa, The influence of particle size distribution on the conversion/time profiles under contracting-geometry kinetic regimes, React. Solids 6 (1988) 281–284.
[46] N. Koga, J.M. Criado, Influence of the particle size distribution on the CRTA curves for the solid-state reactions of interface shrinkage type, J. Therm. Anal. 49 (1997) 1477–1484.
[47] N. Koga, J.M. Criado, Kinetic analyses of solid-state reactions with a particle-size distribution, J. Am. Ceram. Soc. 81 (1998) 2901–2909.

[48] R.W. Hutchinson, S. Kleinberg, F.P. Stein, Effect of particle-size distribution on the thermal decomposition of a-lead azide, J. Phys. Chem. 77 (1973) 870–875.
[49] J.H. Taplin, Index of reaction-a unifying concept for the reaction kinetics of powders, J. Am. Ceram. Soc. 57 (1974) 140–143.
[50] F. Kapteijn, J.A. Moulijn, A. Tarfaoui, Temperature programmed reduction and sulphiding, in: J.A., Moulijn, P.W.N.M. van Leeuwen, R.A. van Santen (Eds.), Catalysis: An integrated approach to homogeneous, heterogeneous and industrial catalysis, Elsevier, Amsterdam, 1993, pp. 401–417.
[51] A.N. Kay Lup, F. Abnisa, W.M.A. Wan Daud, M.K. Aroua, Temperature-programmed reduction of silver(I) oxide using a titania-supported silver catalyst under a H2 atmosphere, J. Chin. Chem. Soc. 66 (2019) 1443–1455.
[52] Y.J. Liu, H.F. Kang, L.L. Zhang, C.L. Xue, L.J. Yuan, X.N. Hou, L. Zhang, Z.X. Gao, Non-isothermal reduction kinetics and mechanisms by hydrogen of Cu–Al spinel solid solution, Catal. Commun. 173 (2023) 106570.
[53] G. Munteanu, E. Segal, Sestak-berggren function in temperature-programmed reduction, J. Therm. Anal. Calorim. 101 (2010) 89–95.
[54] H.-Y. Lin, Y.-W. Chen, C. Li, The mechanism of reduction of iron oxide by hydrogen, 400 (2003) 61–67.
[55] W.K. Jóźwiak, E. Kaczmarek, W. Ignaczak, Determination of reduction mechanism by TPR data for FeO-H_2 system, Annales Universitatis Mariae Curie-Skłodowska 62 (2007) 49–58.
[56] B. Janković, B. Adnadević, S. Mentus, The kinetic analysis of non-isothermal nickel oxide reduction in hydrogen atmosphere using the invariant kinetic parameters method, Thermochim. Acta 456 (2007) 48–55.
[57] B. Janković, B. Adnadević, S. Mentus, The kinetic study of temperature-programmed reduction of nickel oxide in hydrogen atmosphere, Chem. Eng. Sci. 63 (2008) 567–575.
[58] P. Scherrer, Bestimmung der größe und der inneren struktur von kolloidteilchen mittels röntgenstrahlen, Nachrichten Von Der Gesellschaft Der Wissenschaften Zu Göttingen, Mathematisch-Physikalische Klasse 2 (1918) 98–100.
[59] T. Allen, Particle size analysis by image analysis, in: T. Allen (Ed.), Powder Sampling and Particle Size Determination, Elsevier, 2003, pp. 142–207.
[60] P. Malet, A. Caballero, The selection of experimental conditions in temperature-programmed reduction experiments, J. Chem. Soc. Faraday Trans. 1 (84) (1988) 2369–2375.
[61] N.B. Singh, R. Singh, N.P. Singh, Organic solid state reactivity, Tetrahedron 50 (1994) 6441–6493.
[62] A. Khawam, D.R. Flanagan, Solid-state kinetic models: basics and mathematical fundamentals, J. Phys. Chem. B 110 (2006) 17315–17328.
[63] S. Arrhenius, Über die reaktionsgeschwindigkeit bei der inversion von rohrzucker durch säuren, Z. Phys. Chem. 4 (1889) 226–248.
[64] H.E. Kissinger, Variation of peak temperature with heating rate in differential thermal analysis, J. Res. Natl. Inst. Stand. Technol. 57 (1956) 217–221.
[65] R. Svoboda, J. Málek, Is the original kissinger equation obsolete today? J. Therm. Anal. Calorim. 115 (2014) 1961–1967.
[66] N.A. Seaton, J.P.R.B. Walton, N. Quirke, A new analysis method for the determination of the pore size distribution of porous carbons from nitrogen adsorption measurements, Carbon 27 (1989) 853–861.
[67] G.M. Davies, N.A. Seaton, V.S. Vassiliadis, Calculation of pore size distributions of activated carbons from adsorption isotherms, Langmuir 15 (1999) 8235–8245.
[68] J.Y. Kim, J.A. Rodriguez, J.C. Hanson, A.I. Frenkel, P.L. Lee, Reduction of CuO and Cu_2O with H_2: H embedding and kinetic effects in the formation of suboxides, J. Am. Chem. Soc. 125 (2003) 10684–10692.
[69] Y. Unutulmazsoy, C. Cancellieri, L. Lin, L.P.H. Jeurgens, Reduction of thermally grown single-phase CuO and Cu_2O thin films by in-situ time-resolved XRD, Appl. Surf. Sci. 588 (2022) 152896.
[70] J.A. Rodriguez, J.C. Hanson, A.I. Frenkel, J.Y. Kim, M. Pérez, Experimental and theoretical studies on the reaction of H_2 with NiO: role of O vacancies and mechanism for oxide reduction, J. Am. Chem. Soc. 124 (2002) 346–354.
[71] H.L. Friedman, Kinetics of thermal degradation of char-forming plastics from thermogravimetry. application to a phenolic plastic, J. Polym. Sci., Part c: Polym. Symp. 6 (1964) 183–195.
[72] Q. Jeangros, T.W. Hansen, J.B. Wagner, C.D. Damsgaard, R.E. Dunin-Borkowski, C. Hébert, J. Van herle, A. Hessler-Wyser, Reduction of nickel oxide particles by hydrogen studied in an environmental TEM, J. Mater. Sci. 48 (2013) 2893–2907.
[73] J. Dang, K.-C. Chou, X.-J. Hu, G.-H. Zhang, Reduction kinetics of metal oxides by hydrogen, Steel Res. Int. 84 (2013) 526–533.
[74] M.K. Shukla, K. Sharma, Assessment of particle size distribution and tensile properties of hybrid epoxy composite reinforced with functionalized graphene and CNT nanofillers, J. Comput. Appl. Res. Mech. Eng. 12 (2022) 1–12.
[75] D. Jelić, J. Penavin-Škundrić, D. Majstorović, S. Mentus, The thermogravimetric study of silver(I) oxide reduction by hydrogen, Thermochim. Acta 526 (2011) 252–256.
[76] J.C. Juarez, R. Morales, Reduction kinetics of Ag_2MoO_4 by hydrogen, Metall. Mater. Trans. B 39 (2008) 738–745.
[77] D. Waldbillig, A. Wood, D.G. Ivey, Thermal analysis of the cyclic reduction and oxidation behaviour of SOFC anodes, Solid State Ion. 176 (2005) 847–859.
[78] H.M. Ahmed, A.H.A. El-Geassy, S. Seetharaman, Kinetics of reduction of NiO-WO_3 mixtures by hydrogen, Metall. Mater. Trans. b. 41 (2010) 161–172.
[79] Q. Jeangros, T.W. Hansen, J.B. Wagner, C.D. Damsgaard, R.E. Dunin-Borkowski, C. Hébert, J. Van Herle, A. Hessler-Wyser, Reduction of nickel oxide particles by hydrogen studied in an environmental TEM, J. Mater. Sci. 48 (2013) 2893–2907.
[80] B.V. L'vov, A.K. Galwey, The mechanism and kinetics of NiO reduction by hydrogen - thermochemical approach, J. Therm. Anal. Calorim. 110 (2012) 601–610.
[81] J.T. Richardson, R. Scates, M.V. Twigg, X-ray diffraction study of nickel oxide reduction by hydrogen, Appl. Catal. A Gen. 246 (2003) 137–150.
[82] J.-S. Lee, B.-S. Kim, Synthesis and related kinetics of nanocrystalline ni by hydrogen reduction of NiO, Mater. Trans. 42 (2001) 1607–1612.
[83] P. Erri, A. Varma, Diffusional effects in nickel oxide reduction kinetics, Ind. Eng. Chem. Res. 48 (2009) 4–6.
[84] J.T. Richardson, R.M. Scates, M.V. Twigg, X-ray diffraction study of the hydrogen reduction of NiO/α-Al_2O_3 steam reforming catalysts, Appl. Catal. A Gen. 267 (2004) 35–46.
[85] K.V. Manukyan, A.G. Avetisyan, C.E. Shuck, H.A. Chatilyan, S. Rouvimov, S. L. Kharatyan, A.S. Mukasyan, Nickel oxide reduction by hydrogen: kinetics and structural transformations, J. Phys. Chem. C 119 (2015) 16131–16138.
[86] T.A. Utigard, M. Wu, G. Plascencia, T. Marin, Reduction kinetics of goro nickel oxide using hydrogen, Chem. Eng. Sci. 60 (2005) 2061–2068.
[87] J. Li, Q. Zhu, H. Li, Relationship between reaction and diffusion during ultrafine NiO reduction toward agglomeration fluidization, AIChE J. 67 (2021) e17081.